LBL-25176
Preprint

Lawrence Berkeley Laboratory
UNIVERSITY OF CALIFORNIA

Physics Division

Mathematics Department

To be submitted for publication

Vortex Methods for Slightly Viscous Three Dimensional Flow

D. Fishelov

April 1988

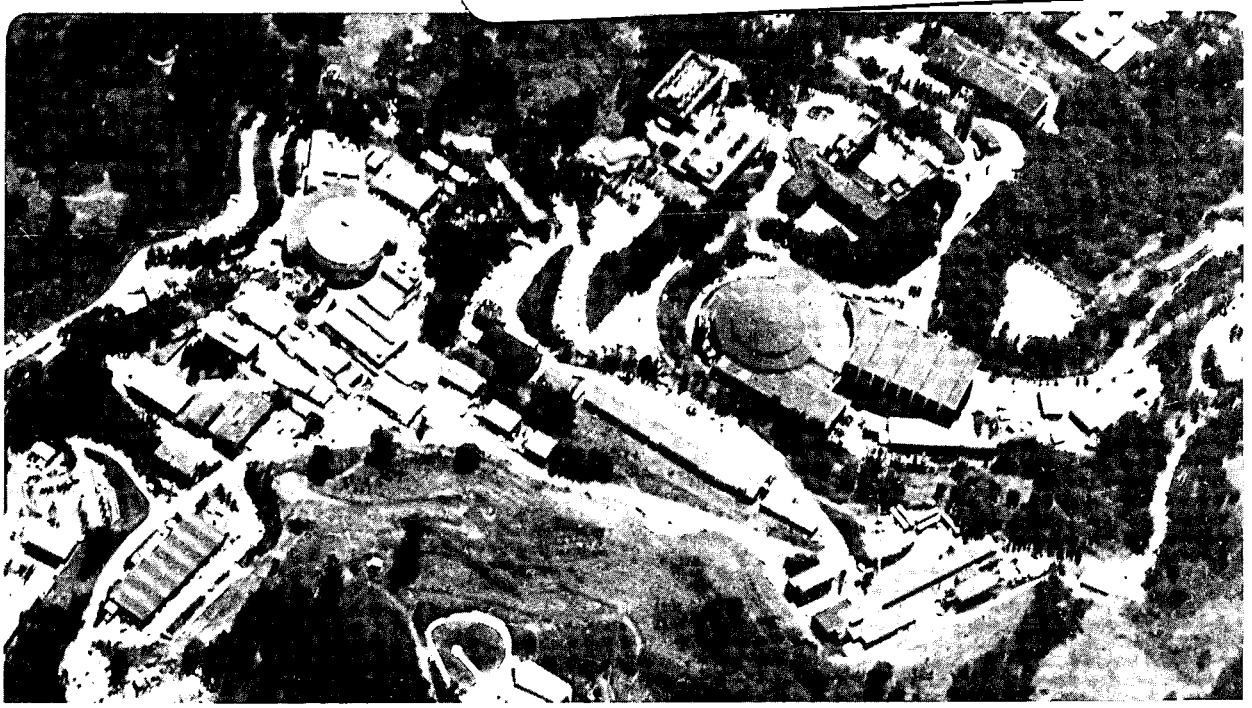

Prepared for the U.S. Department of Energy under Contract Number DE-AC03-76SF00098.

DISCLAIMER

LBL-25176

VORTEX METHODS FOR SLIGHTLY VISCOUS THREE DIMENSIONAL FLOW[1]

Dalia Fishelov

Department of Mathematics
and
Lawrence Berkeley Laboratory
University of California
Berkeley, California 94720, USA

April 1988

[1]Supported in part by the Applied Mathematical Sciences Subprogram of the Office of Energy Research, U.S. Department of Energy under contract DE-AC03-76SF00098.

VORTEX METHODS FOR SLIGHTLY VISCOUS THREE DIMENSIONAL FLOW

Dalia Fishelov

Department of Mathematics and Lawrence Berkeley Laboratory,
University of California, Berkeley, California 94720

Abstract. Vortex methods for slightly viscous three dimensional flow are presented. Vortex methods have been used extensively for two dimensional problems, though their most efficient extension to three dimensional problems is still under investigation. We chose to apply a method that evaluates the vorticity by exactly differentiating an approximate velocity field . Numerical results are presented for a flow past a semi-infinite plate, and they demonstrate three dimensional features of the flow and transition to turbulence.

Key words: Vortex Methods, Boundary layers, Turbulent Flow.
AMS(MOS) Subject Cassifications:76D05, 76D10, 35Q10.

1. Introduction

Vortex methods as suggested by Chorin[11] were applied to various problems to simulate incompressible flows (see [24], [22] for a review). These grid-free methods represent complicated flows by concentrating the computational elements in regions where small scales phenomena predominate and few elements elsewhere. In addition, vortex methods introduce no artificial viscosity, and therefore they are adequate for solving the slightly

viscous Navier Stokes equation.

Vortex methods have been used extensively in the last fifteen years, especially for two dimensional flows. Though three dimensional vortex methods have been considered inherently difficult, we represent a scheme that involves no elaborate computations and is a natural extension of the two dimensional schemes. We applied this method to a three dimensional flow past a semi-infinite plate at high Reynolds number. The velocity far away from the plate is assumed to be uniform. If one assumes that the flow is independent of the spanwise variable, the problem is two-dimensional, otherwise the flow is three dimensional. Chorin ([10], [11], [12]) solved the two dimensional problem numerically; he used computational elements, called blobs, with smoothed kernel. This kernel is obtained by convolving the singular kernel, which connects vorticity and velocity, with a smoothing function (called a cutoff function). The latter approximates a delta function in the sense that a finite number of its moments are identical to those of a delta function.

A numerical solution to a three dimensional problem was introduced by Chorin ([10], 1980) and by Leonard ([22],[23], [24]) using different vortex filament methods. In the filament method one approximates the initial velocity and vorticity along vortex lines, whose tangents are parallel to the vorticity vector. Since circulation is conserved along vortex lines, there is no need to update vorticity. Both authors ([10],[24]) stepped the Navier-Stokes equations in time by splitting them to the Euler and the heat equations. In [23] Leonard introduces one of the earliest vortex methods to solve the inviscid three-dimensional Euler equations numerically. In his computations he was able to simulate the time development of spotline disturbances in laminar three-dimensional boundary layer. He suggested to split the velocity field into a sum of the velocity at infinity and a perturbed one, and to track vortex lines and compute their curvatures. He extended his method to the viscous case ([24]) using a core spreading technique, in which the core of the filaments was changed every time step to satisfy the heat equation. This scheme was proved to

approximate the wrong equations, rather than the Navier-Stokes equations ([16]).

Chorin suggested a different filament method to solve the three-dimensional problem. He approximates vortex lines by segments and then, using the Biot-Savart law, he updates the endpoints of the segments for the Euler equation every time step. The heat equation is approximated in the statistical sense via a random-walk algorithm. Since Chorin uses segments to approximate vortex lines, his algorithm involves no elaborate calculations, such as evaluation of curvatures. However it is not highly accurate in space. The purpose of this paper is to modify Chorin's scheme to gain higher spatial accuracy.

Following Beale and Majda ([4],[5]) and Anderson ([1],[2]), we achieve higher spatial accuracy by generalizing the two dimensional blobs to three-dimensional ones. Vorticity as well as blob locations must be updated every time step. Two versions of the three-dimensional blob extension were suggested. Beale and Majda suggested to approximate spatial derivatives with finite differences, while Anderson explicitly differentiates the smoothed kernel mentioned above. We chose to apply the method of Anderson, since it eliminates one source of error, associated with spatial differentiation. The algorithm and its accuracy is then similar to the two-dimensional one. The results shown here are the first attempt to apply this scheme numerically. Convergence was proved in [3] and [9] for the Euler equations. Applying the convergence proofs to our scheme, we show that for smooth cutoff functions second order accuracy in space is gained. Higher order space accuracy can be achieved by using cutoff functions, in which more moments agree with those of a delta function. We were able to resolve three dimensional features of the flow and transition to turbulence. The numerical results are in agreement with experimental results shown in [19], which suggest that at high Reynolds numbers there exist a large number of small hairpins.

The paper is organized as follows. In section 2 we represent the fundmental equations,

in section 3 the numerical scheme, and in section 4 we describe the boundary conditions. In section 5 we show that if one uses a smooth cutoff function, second-order space accuracy is assured for the Euler equations. The error from the viscous term is discussed as well. We also suggest a new way for treating this term. Section 6 represents numerical results and section 7 concludes the paper.

2. Representation of the Problem

The flow is described by the Navier Stokes equations, formulated for the vorticity ξ:

$$\begin{aligned} &\partial_t \xi + (\mathbf{u}\cdot\nabla)\xi - (\xi\cdot\nabla)\mathbf{u} = R^{-1}\Delta\xi, \\ &\text{div } \mathbf{u} = 0, \end{aligned} \tag{2.1}$$

where $\xi = \text{curl } \mathbf{u}$, $\mathbf{u} = (u, v, w)$ is the velocity vector, $\mathbf{r} = (x, y, z)$ is the position vector and $\Delta = \nabla^2$ is the Laplace operator. $R = UL/\nu$ is the Reynolds number, where U and L are typical velocity and length, respectively, and ν is the viscosity.

We will solve the above equations for a flow past a semi-infinite flat plate located at $z = 0$, $x \geq 0$. Far away from the plate (for $z \to \infty$) there is a uniform flow in the positive x direction, i.e.,

$$\mathbf{u} = (U_\infty, 0, 0) \quad \text{for} \quad z \to \infty, \quad t > 0.$$

On the plate we impose the no-leak boundary condition $\mathbf{u}\cdot\mathbf{n} = 0$, where $\mathbf{n}$ is a normal to the plate. We also impose the no-slip boundary condition $\mathbf{u}\cdot\mathbf{s} = 0$, where $\mathbf{s}$ is tangential to the plate. Initially $\mathbf{u} = (U_\infty, 0, 0)$ at $t = 0$.

The Prandtl equations are known to approximate the Navier-Stokes equations near the plate, and are used therefore in a thin layer $0 \leq z \leq z_0$. The Navier Stokes equations are employed in the region $z \geq z_0$. In the Prandtl equations one assumes that $\xi = (\xi_1, \xi_2, 0)$, i.e., ξ_3 is negligible in comparison to the other components (see e.g. [28]). Thus

$$\begin{cases} \partial_t \xi_1 + (\mathbf{u} \cdot \nabla)\xi_1 = R^{-1}\partial_{zz}^2 \xi_1 \\ \partial_t \xi_2 + (\mathbf{u} \cdot \nabla)\xi_2 = R^{-1}\partial_{zz}^2 \xi_2 \\ \text{div } \mathbf{u} = 0 \end{cases} \tag{2.2}$$

$$\xi_1 = -\frac{\partial v}{\partial z}, \quad \xi_2 = \frac{\partial u}{\partial z}, \mathbf{u} = (u, v, w). \tag{2.3}$$

The Prandtl equations admite the two-dimensional steady state solution - the Blasius solution. However, the three-dimensional Navier-Stokes equations are unstable at high Reynolds numbers($R \geq 1000$), i.e., small perturbations in the Blasius solution may cause large perturbations in the solution as time progresses. Once the disturbances in the Blasius solution begin to grow, spanwise vortices appear, the solution then depends on the spanwise variable y, and there is a transition to turbulence. Theoretical aspects of this instability are given in Benney and Lin ([8]) and Benney ([7]); they suggest that the secondary motions produced by the interaction of three-dimensional modes with two-dimensional ones can produce profiles that are highly unstable. Physical experiments done by Kline et al. ([21]), Klebanoff et al. ([20]), and Head and Bandyapodhyay ([19]) showed that secondary motion, caused by the production of longitudinal vorticity due to three-dimensional disturbances, creates highly unstable profiles leading to turbulent spots. Klebanoff et al.([20]) suggested that the weak three-dimensional disturbances may control the nonlinear development of the flow and its transition to turbulence. The experiments of Head and Bandyapodhyay ([19]) for high Reynolds numbers ($R \geq 1000$) indicate the existence of large number of vortex pairs or hairpin vortices, extending through at least a substantial part of the boundary-layer thickness; for the most part they are inclined to the wall at a characteristic angle of 40^0 to 50^0. At low Reynolds numbers ($R \leq 800$) the hairpins are much less elongated and are better described as horseshoe vortices or vortex loops. Head and Bandyapodhyay [19] note that almost all investigators have used experimental techniques that limit the observations to relatively low Reynolds numbers, where the structure is markedly different from that at high Reynolds numbers; vortex lines tend to appear as low aspect-ratio loops rather than extended vortex pairs or hairpins.

One of the conclusions from the experimental data in [21] is that the flow is periodic in the spanwise direction. We therefore solve (2.1) and (2.2) with the following periodic boundary condition.

$$\mathbf{u}(x, y+q, z) = \mathbf{u}(x, y, z)$$

$$\xi(x, y+q, z) = \xi(x, y, z).$$

As was noted in [10], q was found to be roughly 0.1.

3. The Numerical Scheme

We first describe the random-vortex method for the Navier-Stokes equations and then the three-dimensional sheet method, called the tile method, for the Prandtl equations.

Time discretization

We split the Navier-Stokes equations into the Euler equations and the heat equation. The Euler equation (3.1) governs the flow of an inviscid fluid:

$$\partial_t \xi + (\mathbf{u} \cdot \nabla)\xi - (\xi \cdot \nabla)\mathbf{u} = 0. \tag{3.1}$$

Note that for a two-dimensional case the last term in the left-hand side of (3.1) vanishes, and therefore vorticity is a material property, i.e., $\frac{D\xi}{Dt} = \frac{\partial \xi}{\partial t} + (\mathbf{u} \cdot \nabla)\xi = 0$. However, this is not necessarily true in three dimensions.

The heat equation is

$$\frac{\partial \xi}{\partial t} = R^{-1} \Delta \xi \tag{3.2}$$

(it is also called the diffusion equation). Both (3.1) and (3.2) are easier to analyze than the Navier Stokes equations. We apply a Strang-type scheme to step the Navier-Stokes equations in time, using (3.1) and (3.2). This is done in the following way: we represent both problems above in the form

$$\xi_t = A(\xi).$$

For the first one

$$A(\xi) = A_1(\xi) = (\xi \cdot \nabla)\mathbf{u},$$

and for the second

$$A(\xi) = A_2(\xi) = R^{-1}\Delta\xi.$$

For both operators we apply the Modified Euler scheme

$$\xi^{n+1/2} = \xi^n + \frac{\Delta t}{2}A(\xi^n)$$

$$\xi^{n+1} = \xi^n + \Delta t A(\xi^{n+1/2}).$$

Let $L(\Delta t)$ be the operator which acts on ξ^n to yield ξ^{n+1}, i.e.,

$$L(\Delta t)\xi^n = \xi^{n+1} = \xi^n + \Delta t A(\xi^n + \frac{\Delta t}{2}A(\xi^n)).$$

$L_1(\Delta t), L_2(\Delta t)$ are defined as $L(\Delta t)$ with A_1, A_2 replacing A. We finally arrive the following scheme for discretizating (2.1) in time

$$\xi^{n+1} = L_1\left(\frac{\Delta t}{2}\right) L_2\left(\frac{\Delta t}{2}\right) L_2\left(\frac{\Delta t}{2}\right) L_1\left(\frac{\Delta t}{2}\right) \xi^n.$$

According to [15], this scheme is second order accurate in time, is accurate up to order two in the time variable, even in the nonlinear case. The same time discretization was used also in [14].

Spatial Discretization

(a) The Euler equations

For an incompressible fluid the following relation ((3.7) below) between vorticity and velocity holds ([13]). Since div $\mathbf{u} = 0$, there exists a function ψ, called a stream function, such that

$$\mathbf{u} = \nabla \times \psi, \tag{3.3}$$

and one may choose ψ such that div $\psi = 0$. By definition

$$\xi = \nabla \times \mathbf{u}, \tag{3.4}$$

and therefore, from (3.3), we find that

$$\Delta\psi = -\xi. \tag{3.5}$$

Thus we may determine the velocity from the vorticity by first solving the Poisson equation (3.5), and then applying (3.3).

If G is the fundamental solution of the Laplace equation, then

$$\psi = G * \xi = \int G(\mathbf{x} - \mathbf{x}')\xi(\mathbf{x}')d\mathbf{x}', \tag{3.6}$$

where $G(\mathbf{x}) = -1/4\pi|\mathbf{x}|$, $\mathbf{x} = (x, y, z)$, and the integration is taken over the whole three dimensional space. Substituting (3.6) in (3.3), we find

$$\mathbf{u}(\mathbf{x}, t) = \int K(\mathbf{x} - \mathbf{x}')\xi(\mathbf{x}', t)d\mathbf{x}', \tag{3.7}$$

where

$$K(\mathbf{x}) = -\frac{1}{4\pi|\mathbf{x}|^3}\begin{pmatrix} 0 & -z & y \\ z & 0 & -x \\ -y & x & 0 \end{pmatrix}. \tag{3.8}$$

Note that (3.7) is a consequence of incompressibility only.

In vortex methods particle trajectories are followed. Let $\mathbf{x}(\alpha, t)$ be the trajectory of a particle in of the fluid which is at the point α at $t = 0$. For fixed α the trajectory $\mathbf{x}(\alpha, t)$ is obtained from the velocity field $\mathbf{u}$ as a solution of the ordinary differential equation:

$$\frac{d\mathbf{x}}{dt}(\alpha, t) = \mathbf{u}(\mathbf{x}(\alpha, t), t) \quad , \quad \mathbf{x}(\alpha, 0) = \alpha. \tag{3.9}$$

Combining (3.7) and (3.8), we find

$$\begin{aligned} \frac{d\mathbf{x}}{dt} &= \int K(\mathbf{x}(\alpha, t) - \mathbf{x}'(\alpha, t))\xi(\mathbf{x}', t)d\mathbf{x}' \\ &= \int K(\mathbf{x}(\alpha, t) - \mathbf{x}(\alpha', t))\xi(\mathbf{x}(\alpha', t), t)d\alpha'. \end{aligned} \tag{3.10}$$

The last equality is true, since for an incompressible fluid the Jacobian of the transformation $\alpha(t) \rightarrow \mathbf{x}(\alpha, t)$ is the identity.

One must supply initial contions to (3.10). We therefore set the initial velocity and vorticity on a regular mesh

$$\alpha_i = (h_1 i_1, h_2 i_2, h_3 i_3) \quad i = 1, \ldots, n,$$

$$1 \leq i_1 \leq N_1, \quad 1 \leq i_2 \leq N_2, \quad 1 \leq i_3 \leq N_3,$$

and then track these particles in Lagrangian coordinates. To discretize the equations, we set $\xi = \sum_j \xi_j$, where the ξ_j are functions of small support. Let κ_j be the intensity of the $j-th$ particle, i.e., $\kappa_j = \int \xi_j dxdydz$. Then we obtain the following set of ordinary differential equations for the approximate locations of the particles $\tilde{\mathbf{x}}_i$

$$\begin{aligned} &\frac{d\tilde{\mathbf{x}}_i}{dt}(t) = \tilde{\mathbf{u}}_i(t) = \sum_{j=1}^{n} K_\delta(\tilde{\mathbf{x}}_i(t) - \tilde{\mathbf{x}}_j(t))\tilde{\kappa}_j(t) \\ &\tilde{\mathbf{x}}_i(0) = \alpha_i, \end{aligned} \tag{3.11}$$

where $\phi : R^3 \rightarrow R$, $\phi_\delta = \frac{1}{\delta^3}\phi(\mathbf{x}/\delta)$ is the cutoff function, and $K_\delta = K * \phi_\delta$ is a smoothed kernel. K_δ replaces the kernel K (defined in (3.8)), which is singular at $\mathbf{x} = 0$. Here $\tilde{\kappa}_j(t), \tilde{\mathbf{x}}_j(t)$ approximate $\kappa_j(t)$ and $\mathbf{x}_i(t)$ respectively, the exact intensity and particle locations for the Euler equations.

We may write K_δ in the following way:

$$K_\delta(\mathbf{x}) = K(\mathbf{x}) f_\delta(\mathbf{x}), \tag{3.12}$$

where $f_\delta(\mathbf{x}) = \frac{1}{\delta^3} f(\mathbf{x}/\delta)$. If $f(\mathbf{x})$ is chosen to be radially symmetric, the relation between ϕ and f is $\phi(r) = f'(r)/4\pi r^2$ (see [6]). We specify $f(\mathbf{x}) = f(r)$ below

$$f(r) = \begin{cases} 1 & \text{r}\geq 1 \\ \frac{5}{2}r^3 - \frac{3}{2}r^5 & \text{r}<1. \end{cases} \tag{3.13}$$

This function is continuous with its first derivative at $r = 1$. Substituting (3.8) and (3.13) in (3.12) yields

$$K_\delta = -\frac{1}{4\pi|\mathbf{x}|^3}\begin{pmatrix} 0 & -z & y \\ z & 0 & -x \\ -y & x & 0 \end{pmatrix} \quad \text{for} \quad |\mathbf{x}| > \delta,$$

and

$$K_\delta = -\frac{1}{4\pi|\mathbf{x}|^3\delta^3}\begin{pmatrix} 0 & -z & y \\ z & 0 & -x \\ -y & x & 0 \end{pmatrix} \cdot \left(\frac{5}{2}(r/\delta)^3 - \frac{3}{2}(r/\delta)^5\right) \quad \text{for} \quad |\mathbf{x}| < \delta. \tag{3.14}$$

For a three-dimensional Euler Equation vorticity is not a material quantity, and therefore we must track vorticity as well as blob locations. We use the equation

$$\frac{d\xi}{dt} = (\xi \cdot \nabla)\mathbf{u}.$$

Therefore, the evolution of vorticity along particle trajectories is described by the equations

$$\frac{d\xi}{dt}(\mathbf{x}(\alpha,t),t) = (\xi(\mathbf{x}(\alpha,t),t) \cdot \nabla_{\mathbf{x}})\mathbf{u}(\mathbf{x}(\alpha,t),t), \tag{3.15}$$

where $\nabla_{\mathbf{x}}$ is the gradient with respect to the Euleran coordinates. Applying (3.11), we find that the following equality holds for the approximatedvelocity $\tilde{\mathbf{u}}$

$$\nabla_{\mathbf{x}}\tilde{\mathbf{u}}(\mathbf{x},t) = \sum_{j=1}^{n} \nabla_{\mathbf{x}} K_\delta(\mathbf{x} - \tilde{\mathbf{x}}_j(t))\tilde{\kappa}_j(t),$$

where $\nabla_{\mathbf{x}} K_\delta$ is derived analytically in Euleran coordinates using the definition of K_δ (3.15). Substitution of the last equality in (3.14) yields

$$\frac{d\tilde{\kappa}_i}{dt} = \sum_{j=1}^{n} (\tilde{\kappa}_i \cdot \nabla\mathbf{x}) K_\delta(\tilde{\mathbf{x}}_i(t) - \tilde{\mathbf{x}}_j(t))\tilde{\kappa}_j(t). \tag{3.16}$$

This can be written in the form

$$\frac{d\tilde{\kappa}_i}{dt} = \sum_{j=1}^{n} (\tilde{\kappa}_i^x A(\tilde{\mathbf{x}}_i - \tilde{\mathbf{x}}_j)\tilde{\kappa}_j(t) + \tilde{\kappa}_i^y B(\tilde{\mathbf{x}}_i - \tilde{\mathbf{x}}_j)\tilde{\kappa}_j(t) + \tilde{\kappa}_i^z C(\tilde{\mathbf{x}}_i - \tilde{\mathbf{x}}_j)\tilde{\kappa}_j(t)), \tag{3.17}$$

where $\tilde{\kappa}_i = (\tilde{\kappa}_i^x, \tilde{\kappa}_i^y, \tilde{\kappa}_i^z)$, and

$$A(\mathbf{x}) = \frac{\partial}{\partial x} K_\delta(\mathbf{x}), \quad B(\mathbf{x}) = \frac{\partial}{\partial y} K_\delta(\mathbf{x}), \quad C(\mathbf{x}) = \frac{\partial}{\partial z} K_\delta(\mathbf{x}).$$

Or more explicitly

$$\begin{aligned}
\tilde{\kappa}_i^x A(\mathbf{x})\tilde{\kappa}_j &= \frac{\tilde{\kappa}_i^x}{4\pi|\mathbf{x}|^5}(-(|\mathbf{x}|^2 - 3x^2), 3xy, 3xz) \times \tilde{\kappa}_j \\
\tilde{\kappa}_i^y B(\mathbf{x})\tilde{\kappa}_j &= \frac{\tilde{\kappa}_i^y}{4\pi|\mathbf{x}|^5}(3yx, -(|\mathbf{x}|^2 - 3y^2), 3yz) \times \tilde{\kappa}_j \\
\tilde{\kappa}_i^z C(\mathbf{x})\tilde{\kappa}_j &= \frac{\tilde{\kappa}_i^z}{4\pi|\mathbf{x}|^5}(3zx, 3zy, -(|\mathbf{x}|^2 - 3z^2)) \times \tilde{\kappa}_j,
\end{aligned} \tag{3.18}$$

for $|\mathbf{x}| < \delta$, and

$$\begin{aligned}
\tilde{\kappa}_i^x A(\mathbf{x})\tilde{\kappa}_j &= \frac{\tilde{\kappa}_i^x}{4\pi\delta^5}(-(2.5\delta^2 - 1.5|\mathbf{x}|^2 - 3x^2), 3xy, 3xz) \times \tilde{\kappa}_j \\
\tilde{\kappa}_i^y B(\mathbf{x})\tilde{\kappa}_j &= \frac{\tilde{\kappa}_i^y}{4\pi\delta^5}(3yx, -(2.5\delta^2 - 1.5|\mathbf{x}|^2 - 3y^2), 3yz) \times \tilde{\kappa}_j \\
\tilde{\kappa}_i^z C(\mathbf{x})\tilde{\kappa}_j &= \frac{\tilde{\kappa}_i^z}{4\pi\delta^5}(3zx, 3zy, -(2.5\delta^2 - 1.5|\mathbf{x}|^2 - 3z^2)) \times \tilde{\kappa}_j,
\end{aligned} \tag{3.19}$$

for $|\mathbf{x}| > \delta$. To conclude, the semi-discrete three-dimensional scheme that we used for the Euler equations is:

$$\begin{aligned}
&\frac{d\tilde{\mathbf{x}}_i}{dt}(t) = \tilde{\mathbf{u}}_i(t) = \sum_{i=1}^{n} K_\delta(\tilde{\mathbf{x}}_i(t) - \tilde{\mathbf{x}}_j(t))\tilde{\kappa}_j(t), \\
&\frac{d\tilde{\kappa}_i}{dt} = \sum_{j=1}^{n} (\tilde{\kappa}_i \cdot \nabla \mathbf{x}) K_\delta(\tilde{\mathbf{x}}_i(t) - \tilde{\mathbf{x}}_j(t))\tilde{\kappa}_j(t), \\
&\tilde{\mathbf{x}}_i(0) = \alpha_i, \tilde{\kappa}_i(0) = \kappa_i^0,
\end{aligned} \tag{3.20}$$

where K_δ is defined in (3.14), and the second eqution is given in more detail in (3.17)-(3.19). Here κ_i^0 are initial values of the intensities of the computational elements on the initial grid.

(b) The Heat Equation

The second equation to solve is the heat equation

$$\frac{\partial \xi}{\partial t} = R^{-1}\Delta\xi \quad \text{, or} \quad \frac{\partial \mathbf{u}}{\partial t} = R^{-1}\Delta\mathbf{u}.$$

Following Chorin ([10] and [12]) we use the random-walk method to step the heat equation in time, i.e., we move the blobs according to

$$\tilde{\mathbf{x}}_i^{n+1} = \tilde{\mathbf{x}}_i^n + \eta(\Delta t),$$

where $\eta(\Delta t) = (\eta_1(\Delta t), \eta_2(\Delta t), \eta_3(\Delta t))$ and η_1, η_2, η_3 are Gaussian random variables with mean zero and variance $2\Delta t/R$, chosen independently of each other.

Note that we use the trapezoidal rule in (3.11) and (3.16) in order to approximate spatial integrals. The error due to this approximation depends on the derivatives of the integrants, and in particular on the vorticity, i.e., if the vorticity grows so does the error. Therefore, if we find that the vorticity grows while using blobs for the Navier-Stokes equations, we replace a blob which carries a high enough vorticity with several blobs. The new blobs are placed at the same computational point, and share the same total vorticity of the original blob. Since the random walk is used to simulate the heat equation, these blobs will likely find themselves in different locations at the next time step. If one uses filaments, growth in vorticity causes stretching of the filaments. In this case one should split the vortex line into several short ones, and then use some interpolation between the endpoints of the old filament to keep a desired accuracy. This interpolation is an additional source of error, but it can be avoided if one adopts the three dimensional vortex blob method descibed above.

Prandtl Equations

The Prandtl Equations (2.2) used in a thin layer $0 \leq z \leq z_0$ above the plate, were solved numerically by the tile method, which is the three-dimensional extention of the

sheet method (see [10],[12]). This was done to evaluate the boundary conditions on the plate, since it was found in [12],[10], that blobs did not accurately represrnt the velocity field near the boundary. We describe the tile method for a region $0 \leq z \leq \infty$, noting that the boundary conditions at $z = z_0$ will be viewed as those at infinity, seen from the plate.

In the tile method the computational elements are rectangles, parallel to the plate, that represent a jump in the velocity components u, v. Thus (ξ_1, ξ_2) is the intensity of the tile, where $\xi_2 = u_{above} - u_{below}, \xi_1 = v_{above} - v_{below}$. Consider a collection of N tiles T_i, with intensities $((\xi_1)_i, (\xi_2)_i)$, $i = 1, ..., N$ and centers $\mathbf{x}_i = (x_i, y_i, z_i)$. The motions of these tiles are described by (2.3), i.e.

$$\xi_1 = -\frac{\partial v}{\partial z}, \quad \xi_2 = \frac{\partial u}{\partial z},$$

and if one integrates these equations with respect to z, one has

$$u(x, y, z, t) = u_\infty(x, y, t) - \int_z^\infty \xi_2(x, y, z')dz' \tag{3.21}$$

$$v(x, y, z, t) = v_\infty(x, y, t) + \int_z^\infty \xi_1(x, y, z')dz', \tag{3.22}$$

where $u_\infty(x, y, t), v_\infty(x, y, t)$ are the velocity components u, v as $z \to \infty$. By incompressibility and the boundary condition $w(x, y, 0, t) = 0$, we have

$$w(x, y, z, t) = -\partial_x \int_0^z u(x, y, z')dz' - \partial_y \int_0^z v(x, y, dz')dz'. \tag{3.23}$$

Equations (3.21)-(3.23) provides a relation betwwen the vorticity the velocity, which replaces the one given by (3.7) for the interior region.

The above equations can be approximated by

$$u_i = \tilde{u}(x_i, y_i, z_i, t) = u_\infty(x_i, y_i, t) - 1/2(\xi_2)_i - \sum_j (\xi_2)_j d_j f_j, \tag{3.24}$$

$$v_i = \tilde{v}(x_i, y_i, z_i, t) = v_\infty(x_i, y_i, t) + 1/2(\xi_1)_i + \sum_j (\xi_1)_j d_j f_j, \tag{3.25}$$

where $d_j = 1 - |x_i - x_j|/h_1$, and $f_j = 1 - |y_i - y_j|/h_2$ are smoothing functions, the summations in (2.24-2.25) are over all T_j for which $0 \le d_j \le 1$, $0 \le f_j \le 1$, and $z_j \ge z_i$.

Similarly, from (3.23)

$$w_i = \tilde{w}(x_i, y_i, z_i, t) = -(I_+ - I_-)/h_1 - (J_+ - J_-)/h_2,$$

where

$$I_\pm = u_\infty(x_i \pm h_1/2, y_i, t)z_i - \sum_\pm^x (\xi_2)_j d_j^\pm f_j z_j^*,$$

$$J_\pm = v_\infty(x_i, y_i \pm h_2/2, t)z_i + \sum_\pm^y (\xi_1)_j d_j f_j^\pm z_j^*,$$

and

$$d_j^\pm = 1 - |x_i \pm h_1/2 - x_j|/h_1, \quad f_j^\pm = 1 - |y_i \pm h_2/2 - y_j|/h_2, \quad z_j^* = min(z_i, z_j).$$

The sums $\sum_+^x, \sum_-^x$ are over all T_i, such that $0 \le f_j \le 1$, and $0 \le d_j^+ \le 1$, $0 \le d_j^- \le 1$ respectively. Similarly the sums $\sum_+^y, \sum_-^y$ are over all T_i, such that $0 \le d_j \le 1$, and $0 \le f_j^+ \le 1$, $0 \le f_j^- \le 1$ respectively. This is a thin vertical layer, and therefore the number of operations to calculate the velocity fields for the tile method is $O(N)$.

For simplicity, we describe the motion of a tile for a first order time stepping Euler scheme

$$x_i^{n+1} = x_i^n + \Delta t \cdot u_i,$$

$$y_i^{n+1} = y_i^n + \Delta t \cdot v_i,$$

$$z_i^{n+1} = z_i^n + \Delta t \cdot w_i + \eta(\Delta t),$$

where η is a Gaussian random variable with mean 0 and variance $2\Delta t/R$. Note that η appears only in the z component, since the Prandtl equation (2.2) assumes that vorticity diffuses in the z direction only.

4. Boundary Conditions

We first specify the boundary conditions for the region $z \geq z_0$, in which the Navier-Stokes equations are used. At infinity the flow is uniform and is in the x direction, i.e., $\mathbf{u}(x,y,z,t) \to (U_\infty, 0, 0)$ as $z \to \infty$. Boundary conditions also have to be imposed at $z = z_0$ (see [28], pp. 111), and they link the two computational regions. If a tile finds itself in the region $z \geq z_0$ after taking a time step, it turns into a blob. Similarly, if a blob enters the thin layer in which the Prandtl equations are employed, it becomes a tile. We assign the same circulation to a tile which turns into a blob and vise versa. Thus $\kappa_i = \xi_i h_1 h_2$, where κ_i is the intensity of the blob, and ξ_i is the intensity of the tile. In addition, we require continuity of u and v at $z = z_0$.

The boundary conditions for the Prandtl equations are:

(a) $u(x,y,z_0,t) = u_\infty(x,y,t)$, and $v(x,y,z_0,t) = v_\infty(x,y,t)$, where $u_\infty(x,y,t)$ and $v_\infty(x,y,t)$ are calculated by the blobs, located at $z \geq z_0$,

(b) $\mathbf{u} \cdot \mathbf{n} = 0$ at $z = 0$, where $\mathbf{n}$ is normal to the plate. This is done by the method of images, i.e., for each blob or tile at (x,y,z), carrying vorticity $\xi(x,y,z)$ we add an imaginary blob or tile at (x,y,z) with vorticity $-\xi(x,y,z)$.

(c) $\mathbf{u} \cdot \mathbf{s} = 0$ at $z = 0$, where $\mathbf{s}$ is tangential to the plate $z = 0$. This is done by creating tiles at the boundary, assigning vorticity to each of them (see [10]). In more details: we calculate $u_0 = u(x,y,0) = u_\infty(x,y,t) - \int_0^\infty \xi_2 dz$ and $v_0 = v(x,y,0) = v_\infty(x,y,t) + \int_0^\infty \xi_1 dz$, and replace the integrals $\int_0^\infty \xi_2 dz$ and $\int_0^\infty \xi_1 dz$ by the sums $\sum_{j=1}^\infty (\xi_2)_j d_j f_j$ and $\sum_{j=1}^\infty (\xi_1)_j d_j f_j$ respectively. The only tiles which contribute to these sums are those located in the region $\{\tilde{x}, \tilde{y} |\ |\tilde{x} - x| \leq h_1, |\tilde{y} - y| \leq h_2\}$. If $(u_0, v_0) \neq (0,0)$, new tiles are created at $(x,y,0)$ with equal intensity $\xi = (\xi_1, \xi_2, 0)$, such that $\sqrt{\xi_1^2 + \xi_2^2} \leq \xi_{max}$, where ξ_{max} is a chosen small parameter. As a result the new values of u_0 and

v_0 , denoted by $\tilde{u}_0$ and $\tilde{v}_0$, satisfy

$$|\tilde{u}_0| \leq \xi_{max}, \ |\tilde{v}_0| \leq \xi_{max}. \tag{4.1}$$

Periodic boundary conditions were imposed in the following way. For each blob or tile located at (x, y, z) two other imaginary blobs or tiles were added at $(x, y \pm q, z)$. To save computational time, further blobs or tiles was not added, as their contribution to the flow quantities became smaller the further they are from the computational domain.

We restrict ourselves to the domain $0 \leq x \leq X_0$, rather than $0 \leq x \leq \infty$. Thus we remove any blob or tile whose x - component location exceeds X_0. This is reasonable, since blobs and tiles located far away from the region of interest contribute little to the overall flow. In addition, this procedure economize the cost of computation, for otherwise a large number of computational elements became bunched near $x = X_0$.

5. Convergence

The first convergence proof for vortex methods was given by Hald ([18]) for the two-dimensional Euler's equations. Convergence for the three-dimensional version of vortex method that was suggested by Beale and Majda, for which spatial derivatives are approximated by finite differences, was given in [4],[5],[2]. For our scheme, in which explicit differentiation is applied to approximate spatial derivatives, convergence was first proved by Beale[3], and then, using a different approach, by Cottet[9]. We quote the theorem appearing in [9], since it applies to a slightly more general case, i.e., the restriction $d \geq 4$, where d appears in (5.3)-(5.4) below, is removed in [9].

Let us first define for $p \in [1, \infty)$ and $m \geq 0$ the Sobolev spaces

$$W^{m,p} = \{f, \partial^\alpha f \in L^p(R^n), |\alpha| \leq m\}$$

and by $\|\cdot\|_{m,p}$ the norm

$$\|f\|_{m,p} = \left(\sum_{0 \le |\alpha| \le m} \|\partial^\alpha f\|_{0,p}^p \right)^{1/p},$$

and for $p = \infty$ the usual modification.

Theorem: Convergence in 3-D ([9]).

Assume that the initial viscosity ξ_0 is smooth enough and that the following conditions holds for the cutoff function ϕ:

$$\phi \in W^{m,\infty}(R^3) \cap W^{m,1}(R^3), \ \forall m > 0; \tag{5.1}$$

$$\int_{R^3} \phi(\mathbf{x}) d\mathbf{x} = 1, \tag{5.2}$$

$$\int_{R^3} \mathbf{x}^\alpha \phi(\mathbf{x}) d\mathbf{x} = 0, |\alpha| \le d-1, \tag{5.3}$$

$$\int_{R^3} |\mathbf{x}|^d \phi(\mathbf{x}) dx < \infty; \tag{5.4}$$

and that there exist constants C and $\beta > 1$ such that

$$h \le C\delta^\beta. \tag{5.5}$$

Then there exists a time τ and a constant C, depending only on ξ_0, such that for h and δ small enough

$$\|\tilde{u} - u\|_{0,p} \le C\delta^d, \quad p \in (3/2, \infty], \quad t \in [0, \tau].$$

We now apply this theorem to our scheme. Using the relation $\phi(r) = f'(r)/4\pi r^2$ derived in [6], we find that

$$\phi(r) = \begin{cases} 0 & \text{r}\ge 1 \\ \frac{15}{8\pi}(1-r^2) & \text{r}<1. \end{cases}$$

It is easy to verify that $\phi(r)$ satisfies (5.2) with $d = 2$. In addition, if one chooses the cutoff function ϕ to be infinitely smooth, second order accuracy is achieved. We would now like view the importance of condition (5.1), in case that the latter is satisfied for finite m only.

The error in vortex methods is usually estimated by bounding the part caused by the regularization of the singular kernel separately, and from the one caused by the discretization of the equations. We therefore write the error in the following form:

$$\mathbf{e} = \tilde{\mathbf{u}} - \mathbf{u} = (\mathbf{u}_\delta - \mathbf{u}) + (\tilde{\mathbf{u}} - \mathbf{u}_\delta) = \mathbf{e}_r + \mathbf{e}_d,$$

where $\mathbf{e}_r$ is the regularization error, caused by replacing the singular kernel K by a smoothed one K_δ, and $\mathbf{e}_d$ is the discretization error.

It was proved in [3],[9, Lemma 5.5] that

$$\|\mathbf{e}_r\|_{0,p} \leq C\delta^d, \quad p \in (3/2, \infty]$$

for some time $t \in [0, \tau]$, provided that (5.2)-(5.4) hold. In addition, as was shown in [9],

$$\|\mathbf{e}_d\|_{0,p} \leq Ch^m/\delta^{m-1}, \tag{5.6}$$

in case that (5.1) holds for every $m > 0$. A generalization of this theorem for finite m was given in [27, pp. 315] for a two-dimensional problem. We have to assume, in addition, that

$$\phi \in W^{m-1,\infty}(R^2) \cap W^{m-1,1}(R^2), \ m \geq 3$$

or $\phi \in W^{m-1,\infty}(R^2)$ for $m \geq 2$ and has compact support. Then for all arbitrarily small $s > 0$ there exists a constant C_s, such that

$$\|\tilde{\mathbf{u}} - \mathbf{u}\|_{0,\infty} \leq C_s\delta^{-s}(\delta^d + h^m/\delta^{m-1}),$$

provided that (5.5) is replaced by $c_2^{-1}\delta^\alpha \leq h \leq c_1\delta^\beta$, with $\alpha \geq \beta > 1$. Therefore, by choosing α, β appropriately one can balance the regularization error with the discretization error. Similar results were proven in [2] for the three dimensional vortex methods suggested by Beale and Majda. In our case $\phi \in W^{1,\infty}(R^3)$ and has compact support, and if one could apply similar results to a three-dimensional problem, the discretization error would

have been $O(h^2/\delta)$. Therefore, for $\delta = Ch^{2/3}$, the error is at most of order $h^{4/3}$. This can be improved by choosing an infinitely smooth cutoff function.

We turn to the accuracy of the random walk used to model viscousity. It is well known that in two dimensions the random walk approximates the heat equation, though without high accuracy. More accurate error estimates were given in [17] for a one dimensional heat equation, using a random-walk method with creation of vorticity, i.e.,

$$P\left(\frac{\|\tilde{u}-u\|_{L^2}}{\|u\|_{L^2}} \leq C_R\left(\frac{\Delta t}{t}+\frac{k}{\sqrt{N}}\right)\right) \geq 1-\frac{1}{k^2},$$

where

$$C_R = \left(1+\frac{1}{R}\right)\left(1+\frac{1+\sqrt{1/R}}{\sqrt{1+1/R}}\right),$$

N in the number of tiles, k is an arbitrary positive number, Δt is the time step, and P denotes probability. Note that C_R is a decreasing function of R.

To increase the accuracy for the heat equation, we intend to study the following possibility. The second order space derivatives appearing in the heat equation may be approximated by explicitly differentiating the smoothed kernel. The latter is done in a similar way to that suggested in [2] for the Euler equations. What we do is substitute (3.7) (a consequence of incompressibility only), into the heat equation, replace K by the smoothed kernel K_δ, and then have

$$\frac{\partial \mathbf{u}}{\partial t} = R^{-1}\Delta \int K_\delta(\mathbf{x}-\mathbf{x}')\xi(\mathbf{x}',t)d\mathbf{x}' = R^{-1}\int \Delta K_\delta(\mathbf{x}-\mathbf{x}')\xi(\mathbf{x}',t)d\mathbf{x}'.$$

This will eliminate the error caused by the statistical process, and will yield a scheme, which is similar in nature to that applied to the Euler equations.

6. Numerical Results

We have to specify the following parameters for our numerical scheme. The initial grid, with spacing h_1, h_2, the time step Δt, the maximum allowed intensity of a newly-created

tile, ξ_{max}, are parameters to be chosen. In addition, the cutoff δ, the thickness of the layer for which the Prandtl equations are used, z_0, and the physical domain $0 \leq x \leq X_0$, in which we keep track of the motion of the computational elements, must be specified. We set $X_0 = 1.5$ (as in [10]). We picked $z_0 = C\sqrt{2\Delta t/R}$ with $C = 1.5$, $\sqrt{2\Delta t/R}$ being the standard deviation of the random walk. We made this choice for z_0 to ensure that a tile, located in the layer $0 \leq z \leq z_0$, will have a high probability of moving out of the tile layer in a few time steps, and will then turn into a blob. We picked the Reynolds number $R = 10^4$, since this was high enough to show the three dimensional effects and the transition to turbulence, as was also observed in the experiments in [19]. Following Chorin [10] we picked h_1/π as the cut-off δ. This is in agreement with the condition in the convergence theorem in section 5, that the cut-off δ should be larger than the typical distance between neighboring particles, the latter being of order $1/\sqrt{R}$ in our problem.

After fixing X_0, z_0, and choosing δ, we had to pick the initial spacing h_1, h_2, ξ_{max}, and the time step Δt. To do this, we first ran the two-dimensional problem, in which the independent variables are x, z, and whose steady-state solution is analytically known to be the Blasius solution. We found out, as was also pointed out in [29], that h_1 and ξ_{max} have primary importance, since they control the number of newly created sheets. The latter determines the number of blobs, and therefore the number of computational elements. If larger numbers of computational elements are used, the error in both interior and exterior regions decreases. We tried the following choices for $h_1, \Delta t$ and ξ_{max}:

(a) $h_1 = \Delta t = 0.20, \xi_{max} = 0.1$

(b) $h_1 = \Delta t = 0.15, \xi_{max} = 0.075$

(c) $h_1 = \Delta t = 0.10, \xi_{max} = 0.050.$

For these sets of parameters we checked the drag, given by the following formula (see

e.g. [30],[10])

$$D(x_0) = \int_0^\infty u(x_0, z)(U_\infty - u(x_0, z))dz, \tag{6.1}$$

and compared it with the Blasius drag $D_0 = 0.6641\sqrt{x_0/R}$. The integral in equation (6.1) was discretized by the trapezoidal rule

$$D_{com} = \sum_{i=0}^{m} c_i u(x_0, i\Delta z)(U_\infty - u(x_0, i\Delta z)\Delta z,$$

where $c_o = c_m = 0.5$, and $c_i = 1$, for $1 \leq j \leq m-1$. Here $m = z_{max}/\Delta z$, where z_{max} is the maximal z, for which computational points where found in the region $|x - x_0| \leq h_1$, and Δz was chosen to be 0.004. The relative error in the drag $|(D(x_0) - D_0(x_0))/D_0(x_0)|$ for $x_0 = 1$ is given in Table 1. In addition, in order to measure the intensity of the noise from the statistical process, we averaged the computed drag every ten iterations, i.e.,

$$D_{avg} = 1/10 \sum_{n=0}^{9} D_{com}(t - n\Delta t) \tag{6.2}$$

and calculated the variance of the instantaneous drag from the averaged one. The variance of the drag is given by the following formula:

$$V(D) = E(|D - (E(D)|^2), \tag{6.3}$$

where $E(X)$ is the expected value of a random variable X. We approximated the expected values $E(X)$ in (6.3) by X_{avg}, where the average is computed as in (6.2). One would like to reduce the statistical noise, and therefore to decrease the variance by choosing the appropriate parameters. The results for the drag and variance in the two-dimensional problem are given in Table 1. The total computational time on a VAX-VMS computer is given in this table as well.

grid	relative drag error	variance	No. of sheets	No. of blobs	Time
(a)	0.52	0.061	95	76	3 min.
(b)	0.21	0.024	139	151	13 min.
(c)	0.14	0.016	344	415	127 min.

Table 1

One can learn from Table 1 that the finer is the grid, the smaller the relative error in the drag, and the smaller the variance. In addition, much more time is required for grid (c) than for grid (b). To make our computations affordable for a longer time in the three-dimensional problem, we chose the three-dimensional grid (b). We also had to specify h_2 for three-dimensional problems. We chose $h_2 = q/4$ for grid (a), $h_2 = q/6$ for grid (b), and $h_2 = q/8$ for grid (c).

We examined the instability of the Blasius solution for high Reynolds numbers in a three-dimensional problem. This was done as follows (see [10]). For $0 \leq t \leq T = 1$ we approximated the Prandtl Equations, whose steady-state is the Blasius solution, using only tiles. In the latter vorticity is a material property and therefore instability can not occur. Note that the numerical solution converges to the Blasius solution as $t \to \infty$ and $h_1, h_2 \to 0$, where h_1, h_2 is the size of the initial grid. We used the results of this scheme at $T = 1$ to be the initial conditions for the Navier Stokes equations. Instability for the Navier Stokes equations is shown, i.e., small perturbations in the Blasius solution cause large changes in the solution. We perturbed the Blasius solution by choosing the following initial condition at infinity:

$$\mathbf{u}(x, y, \infty, T) = \begin{cases} (U_\infty, A, 0) & \text{for } \frac{1}{4}q < y < \frac{3}{4}q \\ (u_\infty, 0, 0) & \text{elsewhere,} \end{cases}$$

where $A = 10^{-3}$. After $T = 1$ we used the scheme described in sections 3 and 4, in which tiles and blobs are present, and therefore instability might occur.

We display all the results at $t = 22.5$. Velocity and vorticity are shown in the following two-dimensional planes: (a) $y = \frac{1}{2}q$, which describes the flow quantities as a function of x

and z; (b) at the two planes $x = 1, 1.4$, which shows the velocity and vorticity as a function of y and z. Notice that as x increases the more apparent are the three-dimensional features, i.e., the dependence on y and the transition to turbulence. This happens since the local Reynolds number $R_x = Ux/L$ increases for larger x.

In Figures 1-3 we display velocity components computed at a regular mesh. Figure 1 shows the x, z components of the velocity at $y = q/2$. In Figures 2-3 the y, z components of the velocity at $x = 1, 1.4$ respectively are displayed. These figures, as well as other figures represented for fixed x, show the three-dimensional features of the flow, i.e., the dependence on y. This is in accordance with results appearing in [25] and [26]; in the latter numerical results were performed for a periodic problem in both x and y. They indicate the three dimensional character of secondary instability, which is consistent with the idea that turbulence is intrinsically three dimensional. Vorticity is represented in the Lagrangian computational grid points in Figures 4-6. In Figure 4 the x, z components of vorticity at $y = q/2$ is displayed. One can see that for larger x the intensity of the vorticity increases, which is one of the features of transition to turbulence, i.e., vorticity is no longer preserved in the Lagrangian system as it is in a two-dimensional problem.

In Figures 5-6 we show the y, z components of vorticity at $x = 1, 1.4$ respectively. Note that for larger x the vorticity is no longer directed in one direction. This is in agreement with the results in [19], which indicate the appearance of small hairpins as the flow develops in the streamwise direction. Figures 7 through 9 show contours of the z-component of vorticity. These figures indicate that for larger x small scales phenomena appear. Figures 10 through 12 show contours of the y-component of vorticity, in which the results are similar to those of the z-component of vorticity.

Table 2 gives the running times on a CRAY X-MP for the different three grids, and for different time levels.

grid	t=3	t=6	t=9	t=12	t=22.5
(a)	0.5 min.	1 min	2 min.	3 min.	6 min.
(b)	7 min.	25 min.	43 min.	1 h. 7 min.	2 h. 13 min.
(c)	2 h. 30 min.				

Table 2: Total computational time to reach t=3,6,9,12,22.5

Tables 3 and 4 show the number of tiles and blobs, respectively, for various times (t=3,6,9,12,22.5) and grids (a,b,c).

grid	t=3	t=6	t=9	t=12	t=22.5
(a)	263	323	344	360	348
(b)	1080	962	1000	926	1098
(c)	4548				

Table 3: Number of tiles

grid	t=3	t=6	t=9	t=12	t=22.5
(a)	205	213	187	183	222
(b)	1051	915	830	947	987
(c)	6948				

Table 4: Number of blobs

We found out that our numerical results agree with the experimental results of [19] in a way that both results indicate the existence of small hairpins at high Reynolds numbers. Note that in other experiments horseshoe vortices rather than small hairpins were found. As was explained in [19], the reason for the different results was that the experimental techniques of other investigators limited the results to low Reynolds numbers.

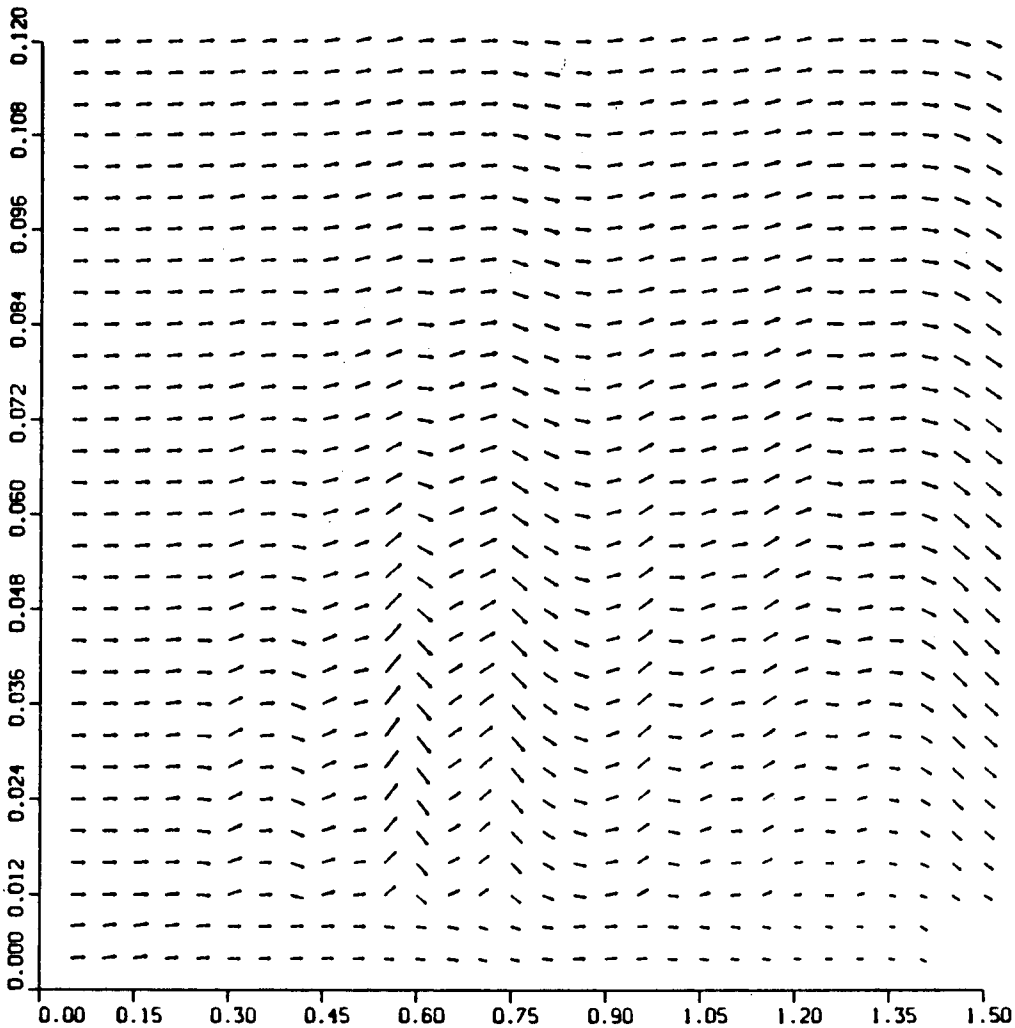

Figure 1. Velocity field in the x, z plane for $y = q/2$.

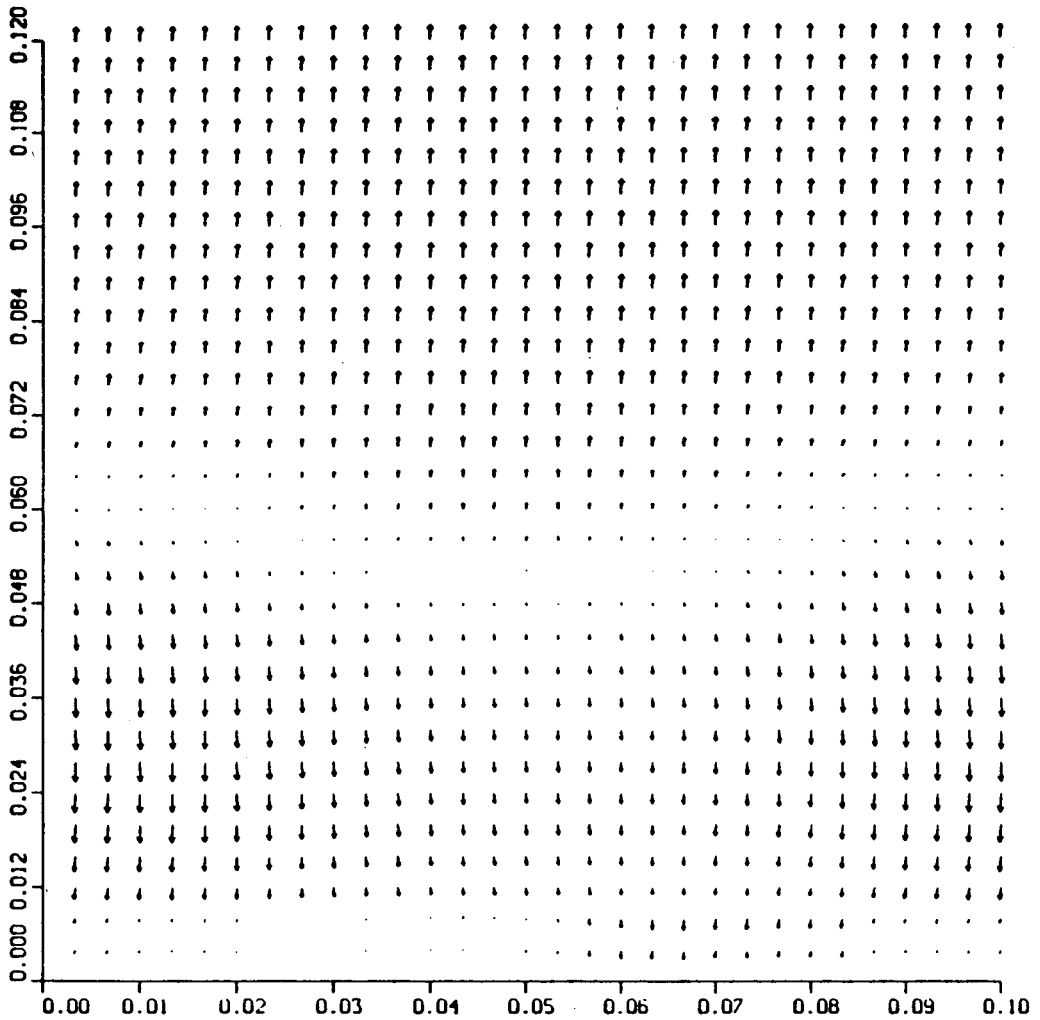

Figure 2. Velocity field in the y, z plane for $x = 1$.

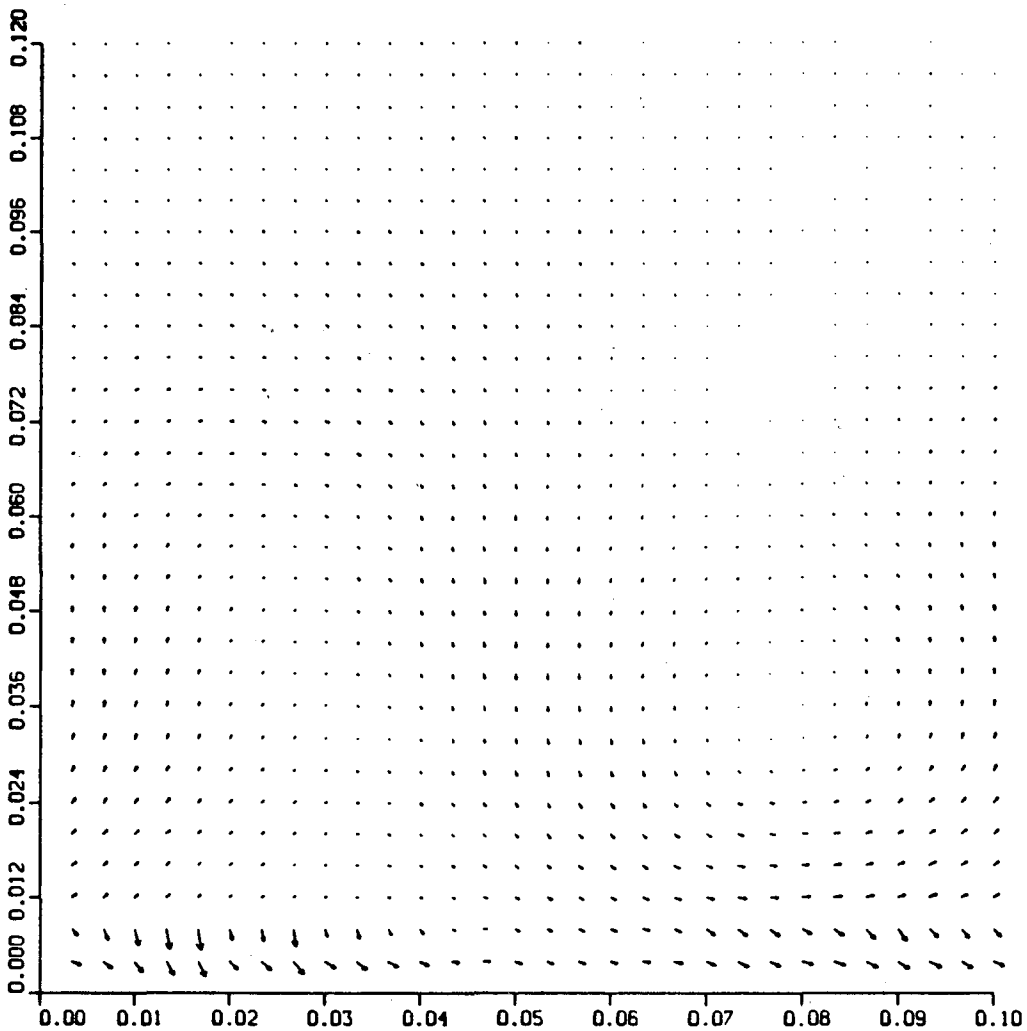

Figure 3. Velocity field in the y, z plane for $x = 1.4$.

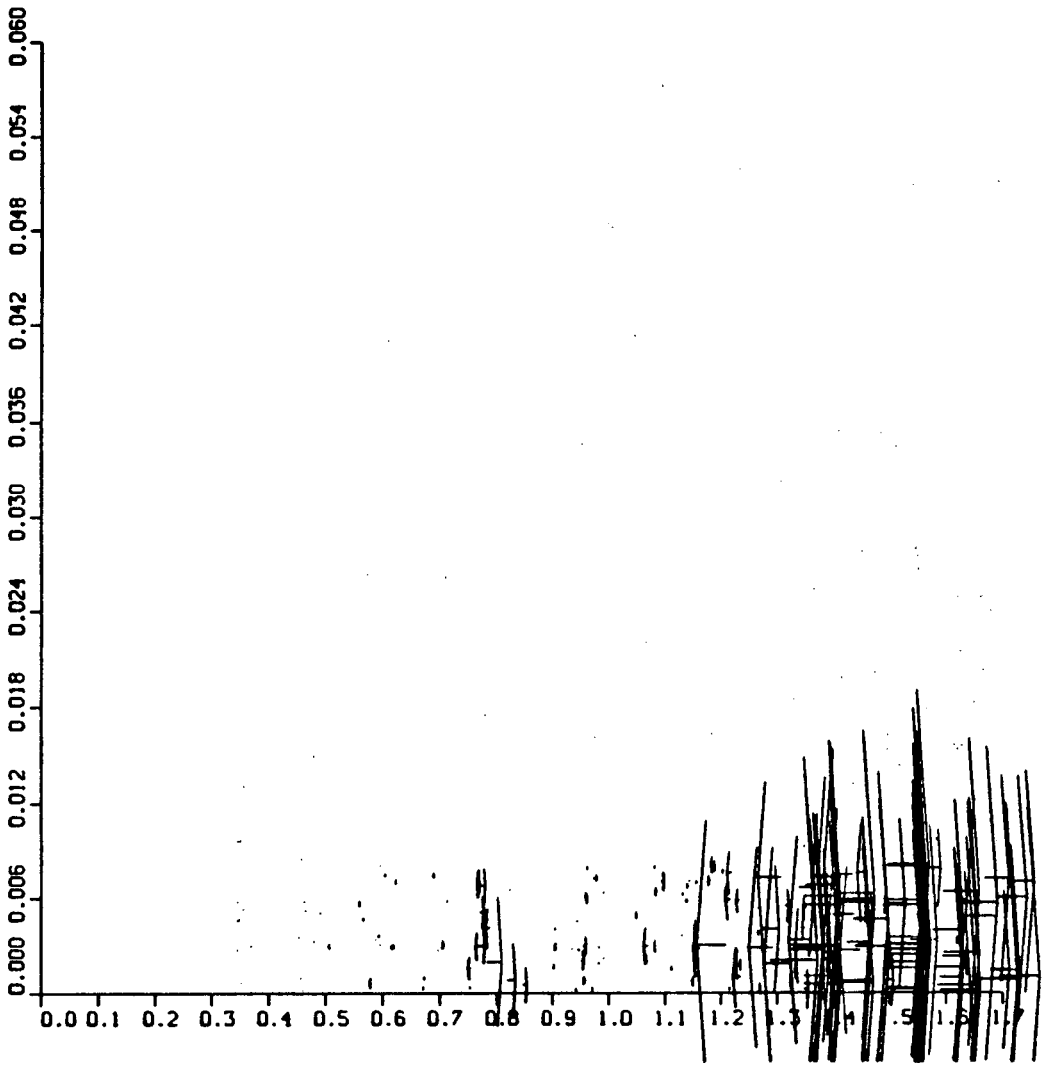

Figure 4. Vorticity in the x, z plane for $y = q/2$.

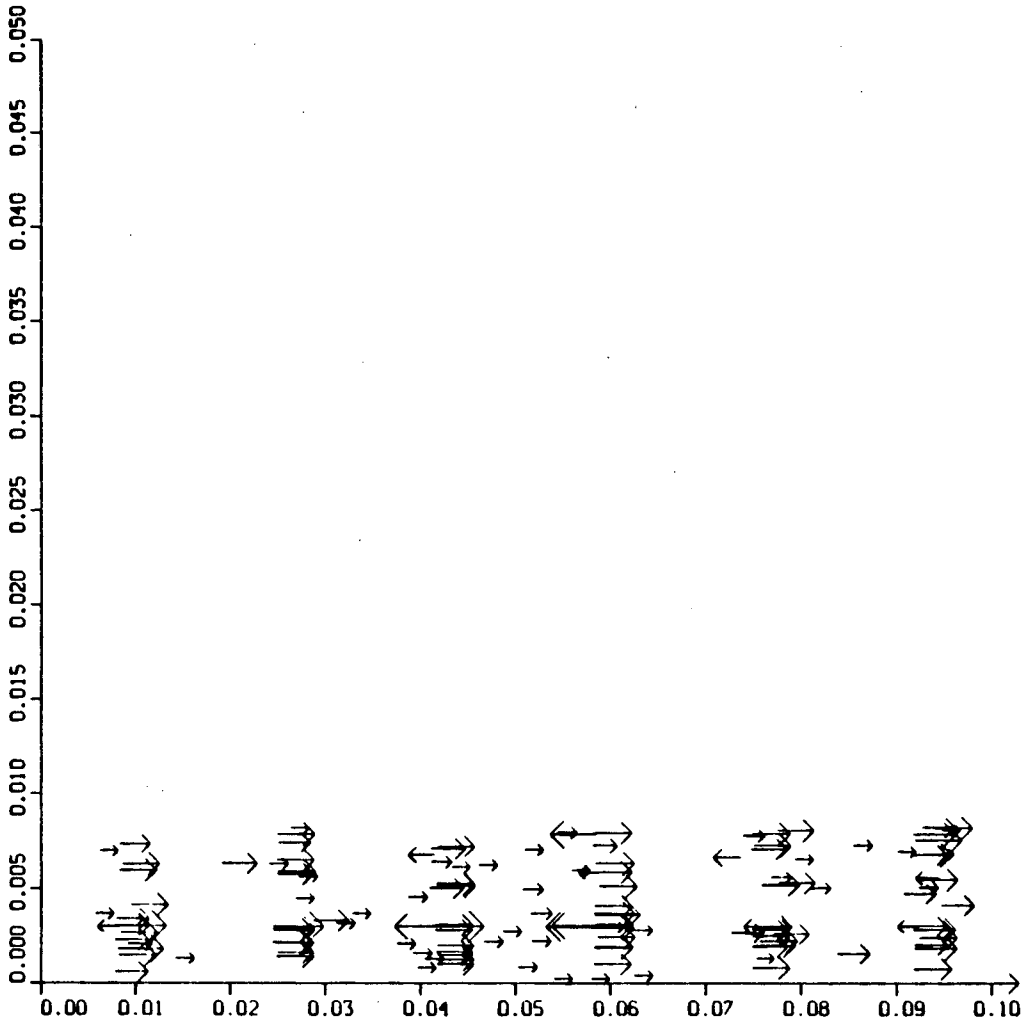

Figure 5. Vorticity in the y, z plane for $x = 1$.

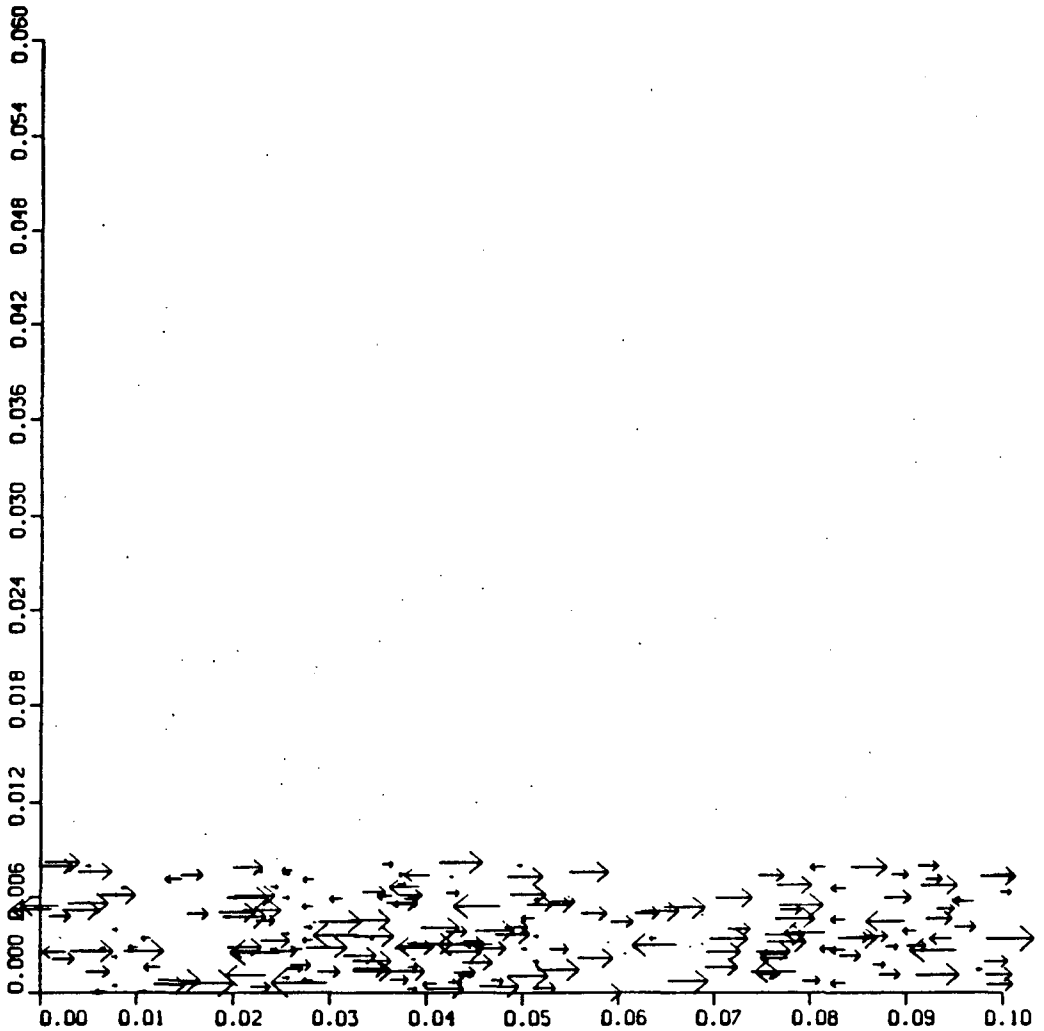

Figure 6. Vorticity in the y, z plane for $x = 1.4$.

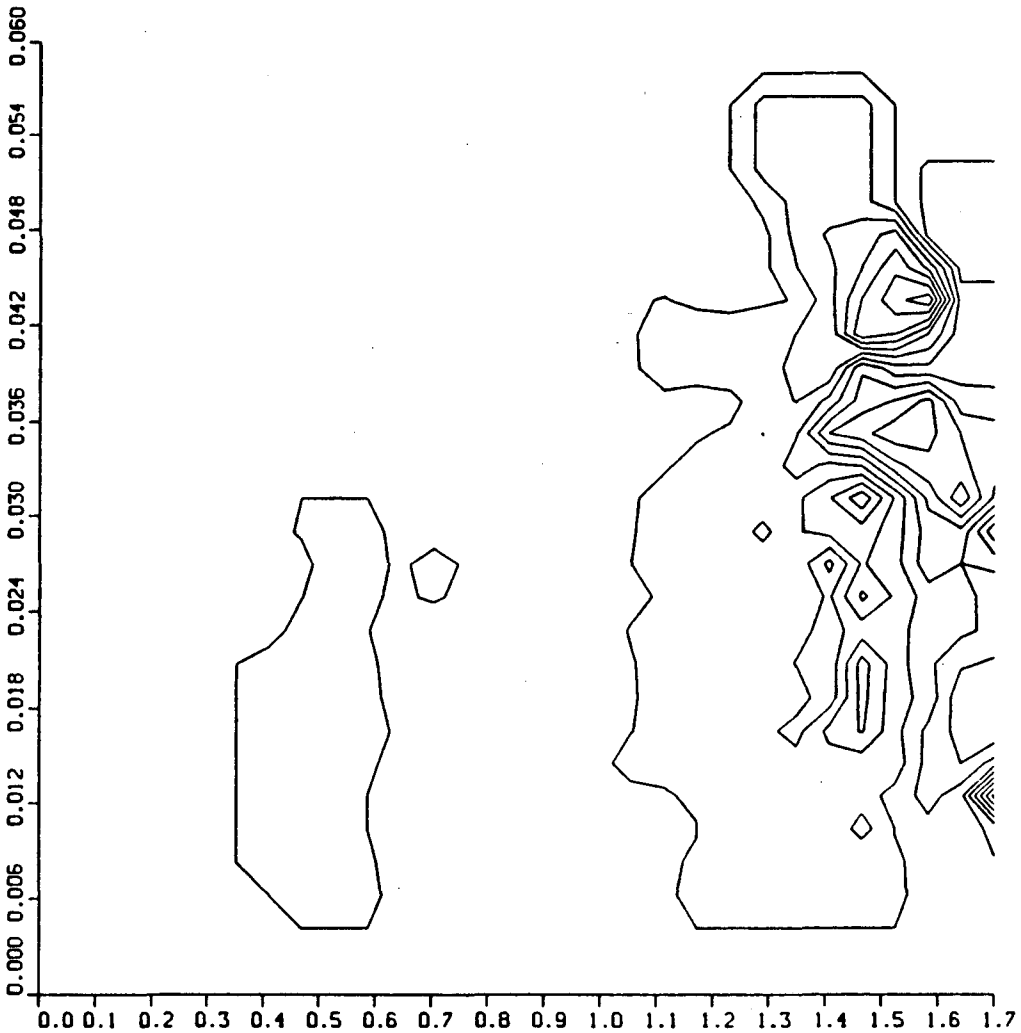

Figure 7. Contours of the z component of vorticity in the x, z plane for $y = q/2$.

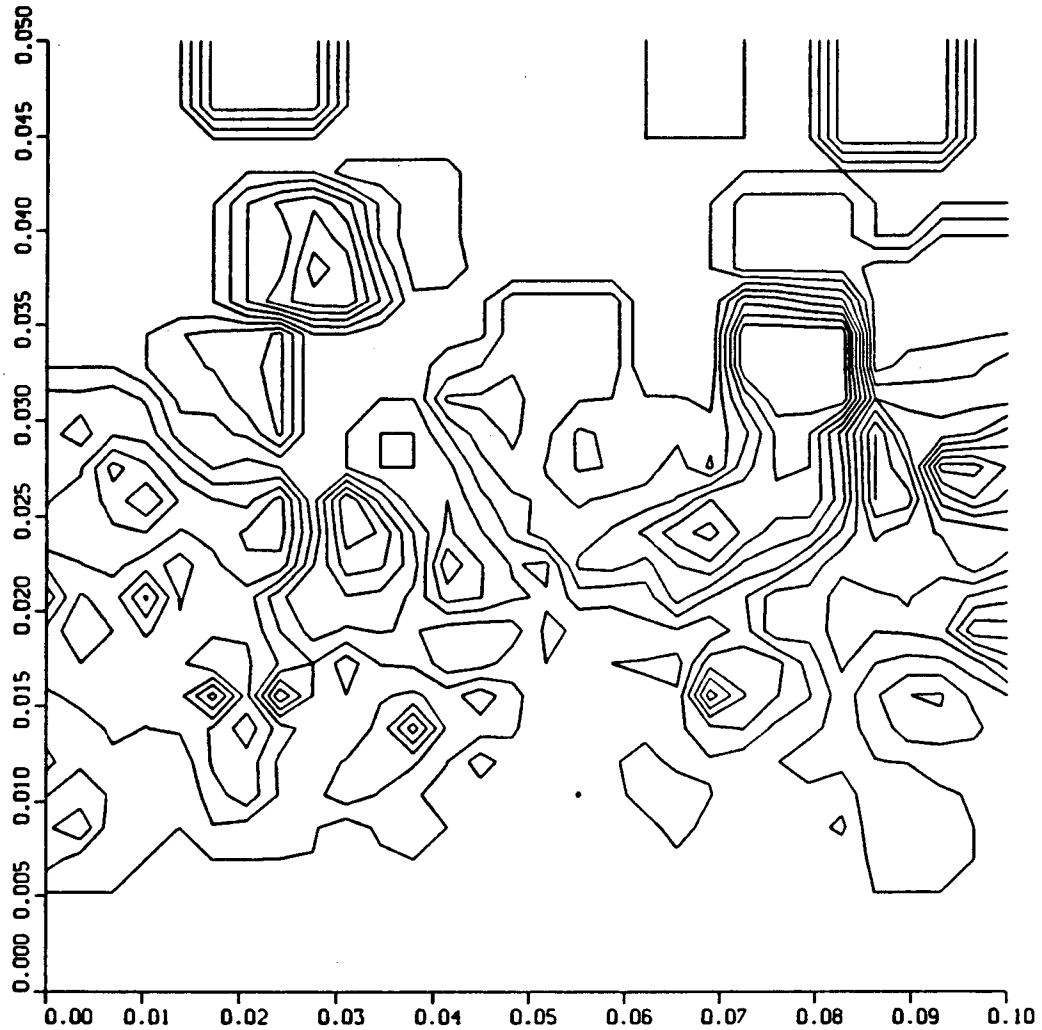

Figure 8. Contours of the z component of vorticity in the y, z plane for $x = 1$.

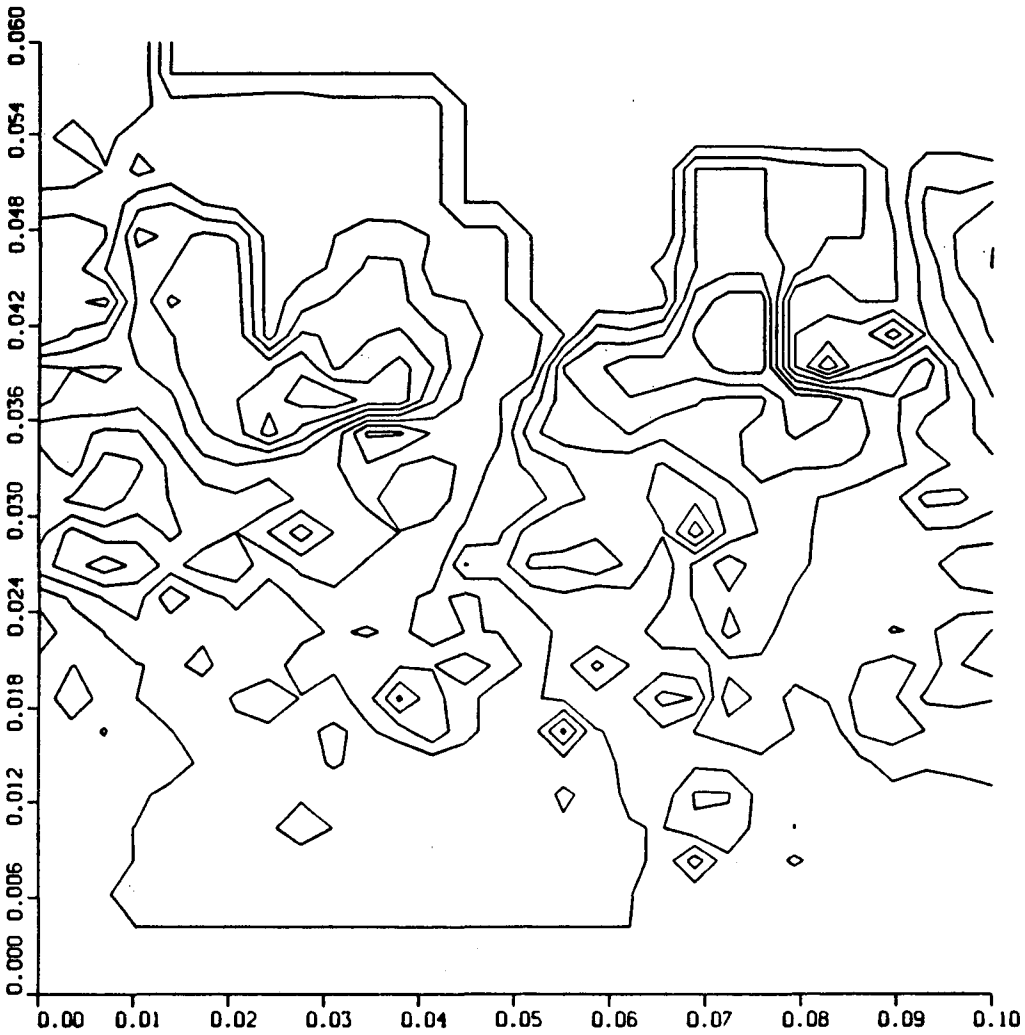

Figure 9. Contours of the z component of vorticity in the y, z plane for $x = 1.4$.

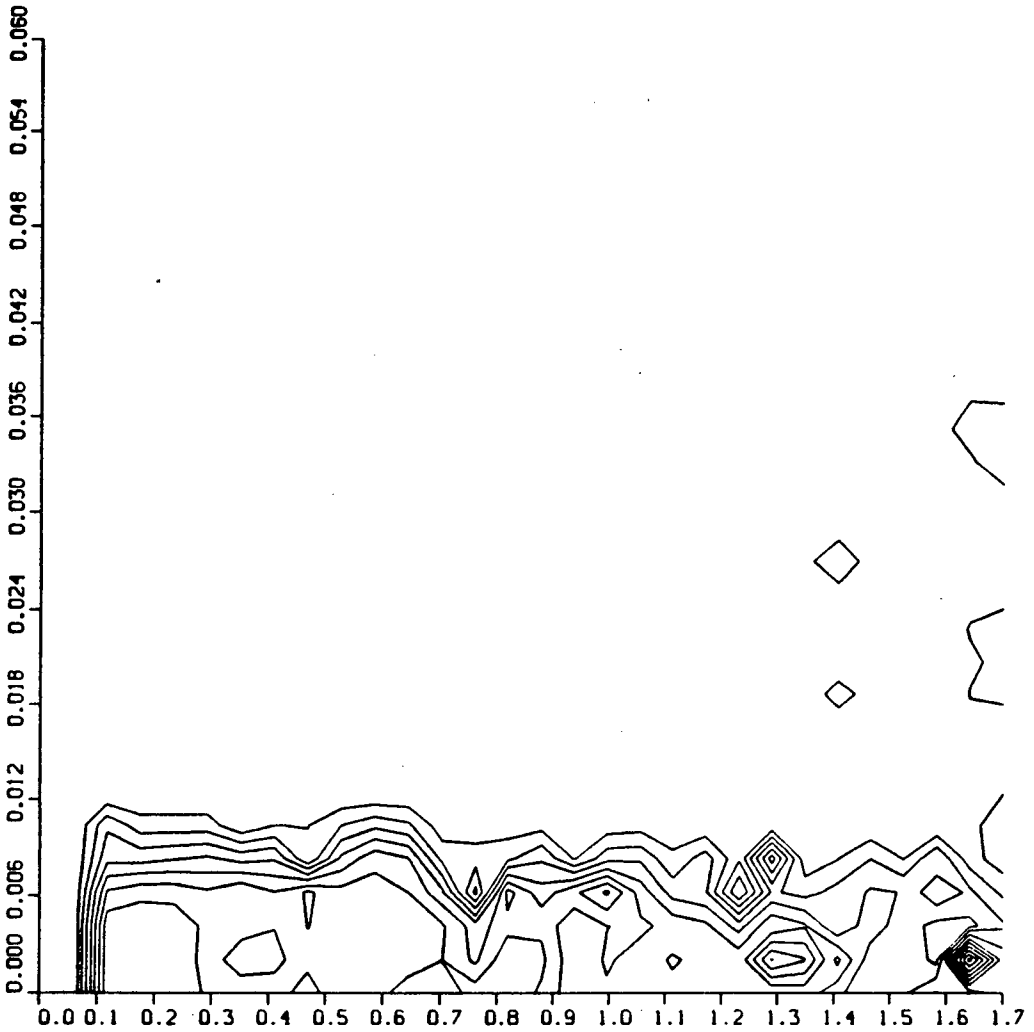

Figure 10. Contours of the y component of vorticity in the x, z plane for $y = q/2$.

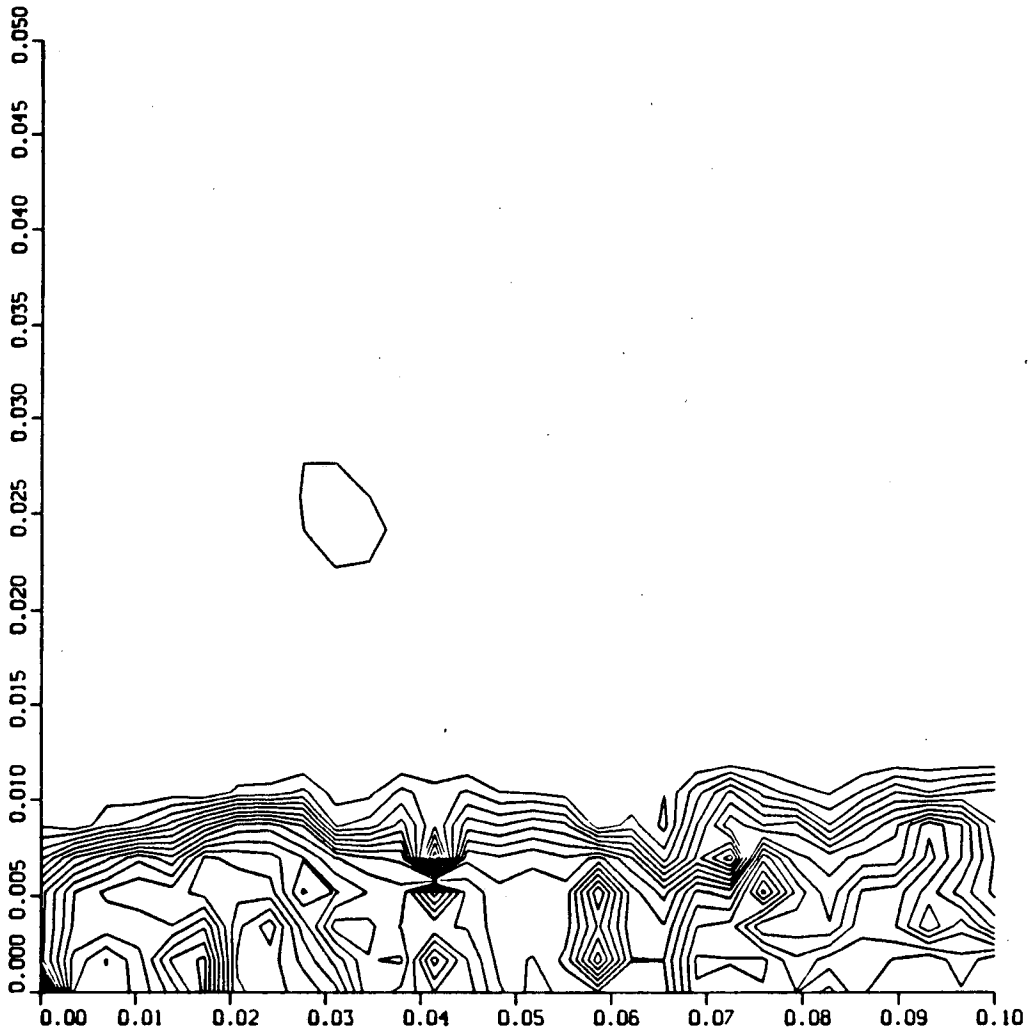

Figure 11. Contours of the y component of vorticity in the y, z plane for $x = 1$.

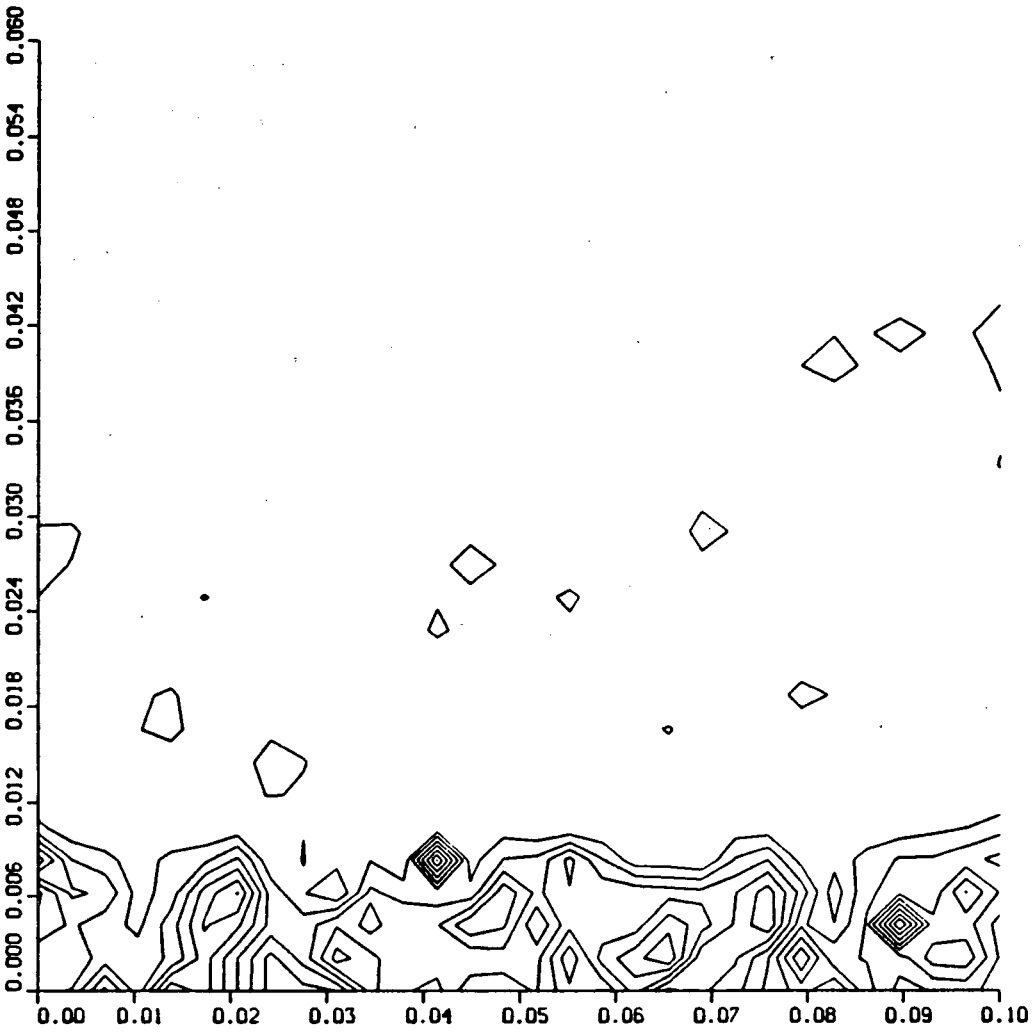

Figure 12. Contours of the y component of vorticity in the y, z plane for $x = 1.4$.

7. Conclusions

The three-dimensional version of vortex methods used here were capable of resolving the three-dimensionality of the flow and the transition to turbulence. Away from the palte, we used a three-dimensional blob method, which is a natural extension of two-dimensional vortex methods. These methods can have high spatial accuracy, and they involve no elaborate calculation. Near the plate, the tile method approximates a thin boundary layer, and is a straightforward extension of the two dimensional sheet method. Therefore the two-dimensional and the three-dimensional problems can be similarly treated numerically.

Acknowledgment

I would like to thank Professor Alexandre Chorin for many helpful discussions. I also wish to thank Dr. Scott Baden for vectorizing the code. This work was supported in part at the Lawrence Berkeley Laboratory by the Applied Mathematical Sciences Subprogram of the Office of Energy Research, U.S. Department of Energy, under contract DE-AC03-76SF00098.

References

[1] C. Anderson, Ph.D. Thesis, UC Berkeley (1983).

[2] C. Anderson and C. Greengard, On vortex methods, SIAM J. Numer. Anal., 22 (1985), pp. 413-440.

[3] T. Beale, A convergent 3-D vortex method with grid-free stretching, Math. Comp., 46 (1986), pp. 401-424.

[4] T. Beale and A. Majda, Vortex methods I: Convergence in three dimensions, Math. Comp., 39 (1982), pp.1-27.

[5] T. Beale and A. Majda, Vortex methods II: Higher order accuracy in two and three dimensions, Math. Comp., 39 (1982), pp. 29-52.

[6] T. Beale and A. Majda, High order accurate vortex methods with explicit velocity kernels, J. Comp. Phys., 58 (1985), pp. 188-208.

[7] D.J. Benney, A nonlinear theory for oscillations in a parallel flow, J. Fluid Mech., 10 (1960), pp.209.

[8] D.J. Benney and C.C. Lin, On the secondary motion induced by oscillations in a shear flow, Phys. Fluids 3 (1960), pp. 650.

[9] G.H. Cottet, A new approach for the analysis of vortex methods in two and three dimensions, To appear in Ann. Inst. Henri Poincare.

[10] A.J. Chorin, Vortex models and boundary layer instability, SIAM, J. Sci. and Stat. Compt., 1 (1980), pp. 1-21.

[11] A.J. Chorin, Numerical study of slightly viscous flow, J. Fluid Mech., 57 (1973), pp. 785-796.

[12] A.J. Chorin, Vortex sheet approximation of boundary layers, J. Comput. Phys., 27 (1978), pp. 428-442.

[13] A.J. Chorin and J.E. Mardsen, A Mathematical Introduction to Fluid Mechanics, Springer-Verlag (1979).

[14] D. Fishelov, Spectral methods for the small disturbance equation of transonic flows, Siam J. Sci. Sta. Comp., Vol. 9, 2 (1988).

[15] D. Gottlieb, Strang type difference schemes for multidimensional problems, Siam J.

Numer. Anal., 9 (1972), pp. 650-661.

[16] C. Greengard, The core spreading vortex method approximates the wrong equation, J. Comp. Phy., 61 (1985), pp. 345-348.

[17] O.H. Hald, Convergence of a random method with creation of vorticity, Siam J. Sci. Stat. Comput., Vol 7 (1986), pp. 1373-1386.

[18] O. Hald and V. Del Prete, Convergence of vortex methods Euler's Equations, Math. Comp., 32 (1978), pp. 791-809.

[19] M.R. Head and P. Bandyapodhyay, New aspects of turbulent boundary layer structure, J. Fluid Mech., 107 (1981), pp. 297-338.

[20] P.S. Klebanoff, K.D. Tidstrom and L.M. Sargent, The three-dimensional nature of the boundary-layer instability, J. Fluid Mech., 12 (1962), pp. 1.

[21] S.J. Kline, W.C. Reynolds, F.A. Schrauband and P.W. Runstadler, The structure of turbulent boundary layers, Ibid., 30 (1967), pp. 741.

[22] A. Leonard, Computing three-dimensional incompressible flows with vortex elements, Ann. Rev. Fluid Mech., 17 (1985), pp. 523-559.

[23] A. Leonard, Vortex simulation of three dimensional spotline disturbances in laminar boundary layer. In Turbulent Shear Flows, 2 (1980), pp. 67-77, Berlin/Heidelberg: Springer-Verlag.

[24] A. Leonard, Vortex methods for flow simulation, J. Comp. Phy., 37, pp. 289-335 (1980).

[25] S.A. Orszag and L.C. Kells, Transition to turbulence in plane Poiseuille and plane

Couette flow, J. Fluid Mech., 96 (1980), pp. 159-205.

[26] S.A. Orszag and A.T. Patera, Secondary instability of wall-bounded shear flows, J. Fluid Mech., 128 (1983), pp. 347-385.

[27] P.A. Raviat, An analysis of particle methods, in Numerical methods in Fluid Dynamics (F. Brezzi ed), Lecture Notes in Mathematics, Vol. 1127, Springer Verlag Berlin (1985).

[28] L.A. Segel, Mathematics Applied to Continuum Mechanics, New York: Mcmillan, 1977.

[29] J.A. Sethian and A.F. Ghoneim, Validation study of vortex methods, J. Comp. Phy., Vol. 74, 2 (1988), pp. 283-317.

[30] H.Shlichting, Boundary Layer Theory, McGraw-Hill, New York (1960).

LAWRENCE BERKELEY LABORATORY
TECHNICAL INFORMATION DEPARTMENT
UNIVERSITY OF CALIFORNIA
BERKELEY, CALIFORNIA 94720